Pol. J. Environ. Stud. Vol. XX, No. X (XXXX), 1-11
DOI: *10.15244/pjoes/211962* ONLINE PUBLICATION DATE: 2025-12-03

Original Research

Valorization of Industrial By-Products and Natural Zeolite for Sintered Materials: Comparative Chemical, Structural, and Thermal Characterization

Ana Stojković[1]*, Ivan Krstić[1], Dragan Đorđević[2], Nenad Krstić[2], Ana Bijelić[1], Milan Protić[1], Amelija Đorđević[1]

[1]Faculty of Occupational Safety, University of Niš, Čarnojevića 10a, Niš, Serbia
[2]Faculty of Sciences and Mathematics, University of Niš, Višegradska 33, Niš, Serbia

Received: 13 July 2025
Accepted: 12 October 2025

Abstract

Valorization of industrial by-products through thermal processes represents an efficient and sustainable solution for waste reduction and the development of new functional materials. This study investigates the potential application of cathode ray tube (CRT) glass, iron slag, fly ash from thermal power plants, and natural zeolite in sintering processes. Characterization was performed using XRF, FTIR, SEM, and TGA methods to examine the chemical, morphological, and thermal properties of the materials. The obtained results indicate complementary chemical and structural characteristics, with SiO_2 and CaO as the dominant components in the analyzed materials. TGA analysis of the mixture, conducted under a controlled temperature regime, simulated the sintering process and demonstrated the thermal compatibility of the materials. In addition to spectroscopy/microscopy, composition-based proxies (basicity, silica modulus, network former/modifier ratio, and rule-of-mixtures density), together with a stable sintering region quantified by TGA (~750-990ºC), were used to appraise sinterability and application-oriented feasibility. The results show that this multicomponent composition enables the optimization of sintered products while preserving structural stability and ensuring negligible mass loss during thermal treatment. The materials analyzed, both individually and in synergy, represent sustainable components for the development of new sintered systems, thereby contributing to advanced recycling technologies and the principles of the circular economy.

Keywords: valorization, cathode ray tube glass, slag, fly ash, zeolite

*e-mail: ana.stojkovic@znrfak.ni.ac.rs
Tel.: +381649787948
ORCID iD: 0000-0002-2043-7424

Introduction

Industrial processes generate substantial amounts of by-products, the inadequate management of which results in negative environmental and economic consequences. The concept of the circular economy, based on the principles of sustainable development, promotes recycling and the reuse of waste materials as alternatives to primary raw materials [1, 2].

Efficient industrial waste management has become a critical factor in extending product life cycles, reducing pollution, and fostering the development of sustainable technologies [3, 4]. In this context, the valorization of industrial by-products through the development of new eco-materials is gaining increased importance. One of the most effective strategies in this domain is sintering – a thermal treatment process that enhances mechanical properties and prolongs the service life of materials [4, 5]. Combining natural materials such as zeolite with industrial waste represents an innovative solution that contributes to sustainability, pollution reduction, and the improvement of final product performance [6, 7].

For this purpose, CRT (cathode ray tube) glass, iron slag, fly ash from thermal power plants, and natural zeolite have been identified as components with high potential for use in sintered systems. The amount of landfilled CRT glass waste is rapidly increasing due to the obsolescence and reduced use of these devices. Globally, more than 6 million tons of waste screens are generated annually, with CRT glass accounting for over half of this waste [8]. Due to its chemical composition and amorphous silica-rich structure, CRT glass is considered suitable for thermal processing and interaction with other components [9, 10]. Moreover, studies have shown that sintering CRT glass eliminates its hazardous properties, resulting in a safe and functional material [11].

Slag, a by-product of iron production, also represents an ongoing waste management issue. It is estimated that between 100 and 150 kg of slag is generated per ton of produced iron, while the total accumulation in global landfills exceeds 1 billion tons [12, 13]. Due to its significant concentrations of SiO_2, Al_2O_3, CaO, Fe_2O_3, and MgO, slag is a suitable raw material for sintered products [14, 15].

Fly ash, a solid by-product generated in thermal power plants, is produced in quantities exceeding 800 million tons annually [16]. Its chemical composition (SiO_2, Al_2O_3, Fe_2O_3, CaO) is similar to that of natural aluminosilicate minerals [17], which enables its broad application as a raw material in the production of construction materials [18], sintered products [19], and others.

Zeolites are natural aluminosilicates characterized by high porosity and ion exchange capacity, making them suitable reference materials in studies of sintered systems [20]. Their application as additives contributes to the enhancement of the structural and functional properties of sintered materials [21].

This study investigates the potential of CRT glass, slag, fly ash, and zeolite for application in sintering processes. The investigation was conducted through chemical, structural, and thermal characterization using XRF, FTIR, SEM, and TGA methods.

The aim of the research is to identify optimal conditions for the valorization of these materials through sintering, based on an analysis of their physico-chemical properties, while simultaneously reducing environmental impact and promoting sustainability in industrial practice. Unlike previous studies, which examined these materials individually, this study evaluates their combined sintering behavior and synergistic thermal performance.

Materials and Methods

For the purposes of this study, the following materials were used: CRT glass, iron slag, fly ash from thermal power plants, and zeolite sourced from the Zlatokop site near Vranjska Banja. The analyses were conducted using XRF, FTIR, SEM, and TGA methods. Prior to testing, all samples were ground into fine powder using a ball mill, then dried in an oven at ~100ºC for 8 h until a constant mass was achieved. The samples were subsequently stored in a desiccator until analysis.

Quantitative and qualitative elemental composition analysis was carried out using X-ray fluorescence (XRF) on a Rigaku Super Mini 200 spectrometer (Rigaku Holdings Corporation, Tokyo, Japan). For the XRF analysis, 2 to 5 g of each material were uniformly pressed into pellets to ensure homogeneous density.

Fourier-transform infrared (FTIR) spectra were recorded using a BOMEM Michelson Hartman & Braun Series MB instrument (Quebec, Canada), within the wavenumber range of 4000-400 cm^{-1} and a resolution of 2 cm^{-1}. Sample preparation followed the standard potassium bromide (KBr) method, in which 1.5 mg of the sample was dispersed in 150 mg of pre-dried KBr. The resulting mixture was vacuum-treated and pressed at 200 MPa to form a transparent pellet.

Surface morphology and microstructure of the samples were examined using scanning electron microscopy (SEM) on a JEOL JSM-5300 microscope (Tokyo, Japan).

Prior to imaging, the samples were coated with a thin layer of conductive material using the sputtering technique in a vacuum to enhance conductivity and image quality.

Thermogravimetric analysis (TGA) was performed using a Perkin-Elmer TGA 4000 analyzer (Norwalk, CT, USA). Before the experiments, instrument calibration was carried out in accordance with the manufacturer's guidelines (temperature, mass, and furnace calibration). Analyses were conducted on approximately 10 mg of sample placed in previously pre-calcined ceramic crucibles. During the analysis, the samples were initially

held at 30ºC for 5 min, then heated to 990ºC at a rate of 15ºC/min, and subsequently maintained isothermally at 990ºC for 60 min. The experiments were conducted in an oxidative atmosphere (oxygen) with a flow rate of 20 mL/min. The data obtained were processed using the Pyris™ software package.

The physical properties of the sintered products were assessed through indirect validation using a benchmarking approach. Consequently, the calculated indices include B (basicity), SM (silica modulus), NFM (network former/modifier), and ROM (rule-of-mixtures) density.

To facilitate the interpretation of XRF results, oxide concentrations were normalized to 100% on an anhydrous basis, excluding loss on ignition (LOI). From these normalized values, several dimensionless composition-based indices were derived in order to characterize the balance between network formers and network modifiers.

$$B = \frac{W(CaO + MgO)}{W(SiO_2 + Al_2O_3)}$$

Index B expresses the relative ratio of alkaline-earth modifiers (CaO, MgO) to network-forming oxides (SiO_2, Al_2O_3), providing an indicator of the degree of depolymerization relative to the stability of the oxide network.

$$SM = \frac{W(SiO_2)}{W(CaO + MgO + Na_2O + K_2O)}$$

In this formulation, SiO_2 is considered the primary network former, while alkaline-earth and alkali oxides act as network modifiers. The ratio emphasizes the degree of network polymerization and is widely applied in slag, glass, and ceramic systems.

$$NFM = \frac{W(SiO_2 + Al_2O_3)}{W(CaO + Fe_2O_3 + MgO + Na_2O + K_2O)}$$

This formulation jointly represents the contribution of SiO_2 and tetrahedral Al_2O_3 as network formers, while CaO, Fe_2O_3, MgO, Na_2O, and K_2O are considered as network modifiers. The inclusion of Fe_2O_3 in the denominator reflects its predominantly depolymerizing effect in multicomponent oxide systems.

$$\rho_{ROM} = \left(\sum_i \frac{x_i}{\rho_i} \right)^{-1}$$

Where x_i is the normalized mass fraction of oxide i and ρ_i are literature densities (g/cm³): SiO_2 = 2.65; Al_2O_3 = 3.98; Fe_2O_3 = 5.24; CaO = 3.34; MgO = 3.58; Na_2O = 2.27; K_2O = 2.35; TiO_2 = 4.23 (W(•) denotes XRF mass percent).

Results and Discussion

In order to evaluate the potential of CRT glass, iron slag, fly ash, and zeolite for application in the sintering process, a comprehensive characterization of the selected materials was conducted. The aim was to determine their chemical composition, identify functional groups, assess morphological features, and evaluate thermal stability prior to sintering. The characterization was performed using the XRF, FTIR, SEM, and TGA method.

XRF Analysis

The results of the chemical composition analysis of the materials, determined by XRF, are presented in Table 1.

Based on the results, it can be observed that silicon dioxide (SiO_2) is the dominant compound in all reference samples, except for slag, where calcium oxide (CaO) prevails.

The analysis of CRT glass confirmed the presence of various metal oxides, with SiO_2 being the most abundant, which is consistent with the findings of Long et al. and Pauzi et al. [22, 23]. As the main component of CRT glass, silicon dioxide acts as a phase mediator during the sintering process. In addition, it lowers the softening temperature and facilitates particle densification, thereby increasing energy efficiency and enabling sintering at lower temperatures [24].

According to the XRF results, CaO is the most dominant compound in the slag sample (46.54%). The high content of calcium and silicon oxides indicates favorable hydraulic and pozzolanic properties. Given the significant silicon content, slag proves to be a suitable raw material for geopolymer synthesis [25]. In the study by Arkame et al., it was emphasized that slag is rich in calcium, silicon, and magnesium and exhibits high mechanical strength and low thermal conductivity, making it suitable for incorporation into sintered structures – findings that align with the chemical composition of the analyzed slag [26]. Accordingly, experimental results show that slag contributes to improved mechanical properties of the sintered product, at an optimal sintering temperature of up to 1200ºC [27].

The chemical analysis of fly ash indicates that silicon dioxide (SiO_2) is the dominant compound, with a mass fraction greater than 50%. Qualitatively, fly ash contains oxides of silicon, aluminum, calcium, and iron, which together account for approximately 90% of the total composition, while the remainder consists of unburned carbon. The most abundant carbon form in fly ash is coke residue, formed through the devolatilization of coal particles. Its subsequent combustion and mineral transformation lead to ash formation in thermal power plants. Fly ash also contains a crystalline phase in a concentration of approximately 50%. Quartz is present in all types of fly ash as a characteristic crystalline component. Additionally, due to the use of lime during combustion, periclase (MgO) also appears in crystalline

Table 1. Chemical composition of the materials analyzed by XRF.

Compound	CRT glass (Wt %)	slag (Wt %)	fly ash (Wt %)	zeolite (Wt %)
SiO_2	60.6	32.20	51.7	71.0
Al_2O_3	2.9	8.30	20.2	13.8
Fe_2O_3	0.6	0.79	11.6	1.0
CaO	1.3	46.54	7.4	8.1
MgO	0.5	7.32	2.4	1.2
K_2O	6.5	0.56	1.0	2.0
Na_2O	7.6	0.35	0.9	0.8
TiO_2	0.3	0.43	1.0	0.2

form in fly ash, further enhancing its functional properties as a component in sintered materials [28].

Based on the qualitative chemical analysis of zeolite, SiO_2 is the most abundant component, while Al_2O_3 and CaO are also present in significant concentrations.

Zeolites are natural aluminosilicates in which aluminum and silicon atoms occupy the centers of tetrahedra composed of four oxygen anions (O^{2-}) [29, 30]. Each oxygen ion in Si–O and Al–O bonds is shared between two neighboring tetrahedral cations [31].

The pores of zeolites are filled with metal cations from groups IA or IIA, as well as water molecules [29]. Due to their high porosity, ion exchange capacity, and specific surface area, natural zeolites are considered highly suitable components for sintered products [31].

FTIR Analysis

To verify the results obtained from XRF analysis, FTIR spectroscopy was performed. The transmission spectra of the analyzed samples are presented in Fig. 1.

In the FTIR spectrum of CRT glass (Fig. 1a)), a band appears at approximately 3400 cm^{-1}, corresponding to the stretching vibrations *v*(OH) of hydroxyl groups from water molecules adsorbed on the sample surface. A characteristic band around 1000 cm^{-1} is attributed to the stretching vibrations *v*(Si–OH) groups, in agreement with the findings of Long et al. [22]. The Si–OH bonds represent strong covalent bonds within the silicate network and are clearly identified in the CRT glass spectra.

Bands at ~450 cm^{-1} and 700 cm^{-1} indicate the presence of metal oxides, consistent with the XRF results [32]. The presence of strong covalent bonds in the silicate network points to chemical stability and potential resistance in sintered systems.

In the spectrum of slag (Fig. 1b)), a weaker band is also observed at ~3400 cm^{-1}, corresponding to the *v*(OH) group vibrations [33]. The band near 1000 cm^{-1} is associated with *v*(Si–O) stretching vibrations, while bands in the region around 450 cm^{-1} and 700 cm^{-1} confirm the presence of metal oxides [34]. This spectrum suggests the coexistence of amorphous and crystalline phases with favorable reactivity for sintering.

The FTIR spectrum of fly ash (Fig. 1c)) shows bands that indicate the presence of carbonyl groups *v*(C=O), likely originating from carbonate minerals, with a characteristic peak at 1650 cm^{-1}. Additionally, bands below 800 cm^{-1} indicate the presence of metal oxides [35], while the prominent band at 1090 cm^{-1} corresponds to the stretching vibrations *v*(Si–O), indicating the presence of silicon in the sample.

The presence of crystalline forms of aluminosilicate glass and quartz is further confirmed by deformation vibrations *δ*(Si–O–Si) and *δ*(Al–O–Si) in the 500-800 cm^{-1} range [36, 37]. This combination of features indicates a high content of mineral phases with pozzolanic potential, beneficial for sintered material applications.

The FTIR spectrum of zeolite (Fig. 1d)) exhibits characteristic bands typical of natural zeolites [38]. An intense and broad band around 3400 cm^{-1} arises from the stretching vibrations *v*(OH) of water molecules, while deformation vibrations of molecularly bound water appear between 1550–1650 cm^{-1}. Bands between 950-1200 cm^{-1} originate from vibrations of structural aluminosilicate units – Si(Al)–O tetrahedral linkages. Internal vibrations of the tetrahedral framework are observed in the 720-650 cm^{-1} region [39]. This analysis confirms that the sample contains natural aluminosilicate minerals with a pronounced crystalline structure. The well-defined band distribution further supports the crystallinity of natural zeolite, indicating its high reactivity and ion-exchange potential for application in sintered systems.

SEM Analysis

The SEM micrographs of the analyzed samples are presented in Fig. 2.

The SEM micrograph of CRT glass (Fig. 2a)) reveals flat and sharp-edged particle contours, resulting from the dry milling process of waste CRT glass.

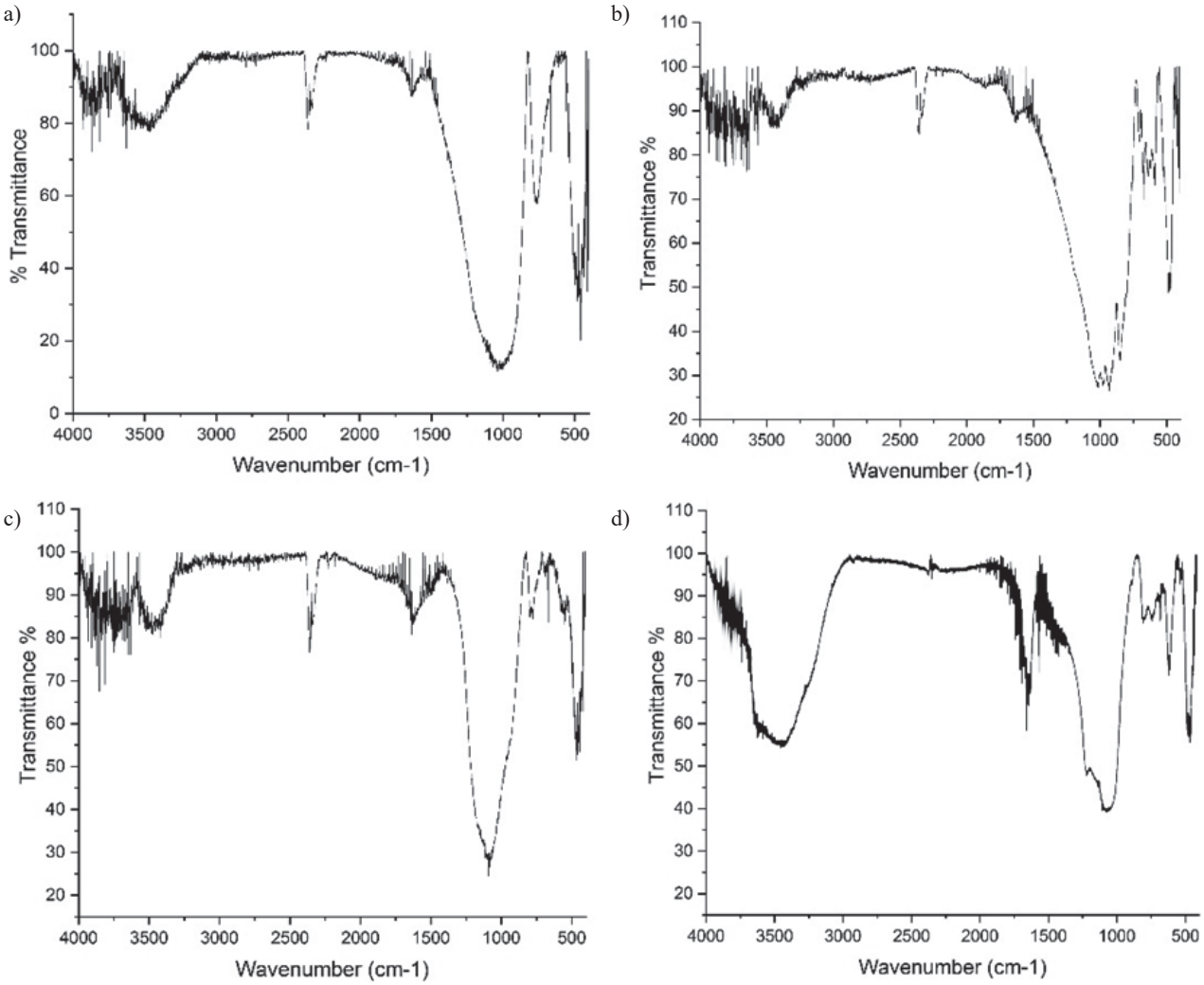

Fig. 1. FTIR of the analyzed samples: a) CRT glass, b) slag, c) fly ash, d) zeolite.

This morphology is consistent with the findings reported by Malchiodi et al. [40]. The particle surfaces appear smooth, which may contribute to improved contact and fusion with other components during the sintering process [22]. Key features of CRT glass as a sintering component – such as thermal stability, low coefficient of linear expansion, chemical inertness, high hardness, and mechanical strength – make it a suitable candidate for incorporation into sintered structures [41].

The micrographs of slag (Fig. 2b)) show predominantly spherical particles, in agreement with the study by Sethupathy et al. [42]. In addition, a pronounced coarse crystalline morphology is observed, with numerous active pores and voids.

Microstructural analysis reveals the presence of cracks, porosity, and interfacial transitions, which significantly influence the behavior of slag during the sintering process [43]. Such morphology is favorable for forming interfacial bonds during sintering, as it facilitates diffusion and bonding between particles, contributing to the strength and stability of the final product.

The SEM analysis of fly ash (Fig. 2c)) shows both amorphous and crystalline phases, with clearly defined spherical particles. The amorphous phase is desirable due to the presence of reactive aluminosilicates, whereas crystalline phases such as quartz, magnetite, and hematite are less reactive at lower temperatures [44]. Particle shapes vary – from regular spheres to irregular and sharp-edged forms. Fly ash is porous and hydrophilic, with its reactivity strongly influenced by particle size. Smaller particles, which cool rapidly after exiting the combustion chamber, possess a disordered and thus more reactive structure. In this study, the analyzed fly ash primarily consists of particles approximately 5 μm and 10 μm in diameter, which can be easily integrated into sintered matrices. The presence of the amorphous phase indicates high pozzolanic potential, while crystalline phases provide additional mechanical stability.

The SEM micrographs of zeolite (Fig. 2d)) exhibit porous and well-defined crystalline structures typical of natural zeolites. Crystals of varying shapes but similar dimensions are observed, with a tendency

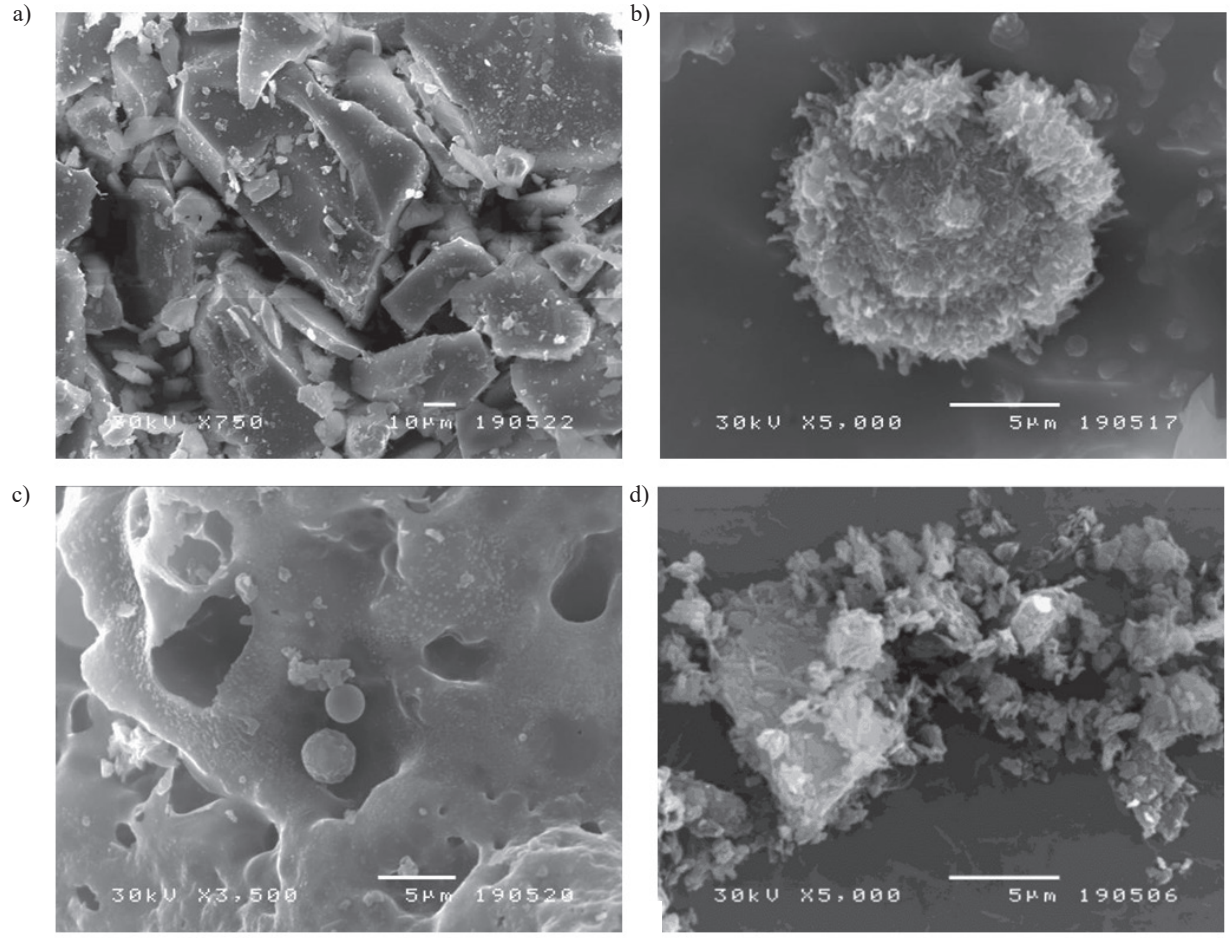

Fig. 2. SEM of the samples: a) CRT glass, b) slag, c) fly ash, d) zeolite.

toward aggregation [29]. These features confirm the presence of structurally stable and active components suitable for incorporation into sintered materials. The microstructure, along with structural uniformity, suggests the ability of zeolite to disperse evenly within the mixture and contributes to enhanced mechanical and thermal properties of the sintered material.

TGA Analysis

TGA and DTG of the samples are presented in Figs 3 and 4.

Thermogravimetric analysis of all materials was conducted according to the following temperature program: samples were first held at 30ºC for 1 min, then heated from 30ºC to 990ºC at a rate of 15ºC/min, and subsequently maintained isothermally at 990ºC for 60 min. This procedure was designed to simulate thermal treatment conditions corresponding to the sintering process.

From the graphs in Figs 3 and 4 (red curve), it is evident that CRT glass exhibited no significant mass change during thermal treatment. The residual mass at 990ºC was 99.14%, indicating high thermal stability. These results are consistent with the study by Isopencu et al. [45], which reported that CRT glass shows an ideal sintering temperature between 800ºC and 900ºC – precisely within the region of negligible mass loss on the TGA curve.

Based on the blue curves (Figs 3 and 4), which represent the TGA and DTG results for slag, no substantial mass loss was recorded either, with a residual mass of approximately 100% at 990ºC. The TGA results suggest that the optimal sintering temperature for slag lies within the range of 800-900ºC.

The green curves (Figs 3 and 4) show the TGA and DTG analysis of fly ash. A residual mass of 98.4% was recorded at 990ºC, with a single mass loss phase (~1.6%) occurring in the temperature range of 475-690ºC. The inflection point at 535.64ºC corresponds to the combustion of residual organic carbon, which typically oxidizes around 550ºC [46]. The unburned carbon content can reach up to 10% and significantly influences the reactivity of fly ash. Additionally, the decomposition of calcium and magnesium carbonates is expected around 650ºC. Due to its richness in amorphous SiO_2, Al_2O_3, and Fe_2O_3, fly ash exhibits pronounced pozzolanic properties, confirming its effectiveness as a sintering component [47].

The purple curves (Figs 3 and 4), corresponding to the TGA and DTG analysis of zeolite, reveal two

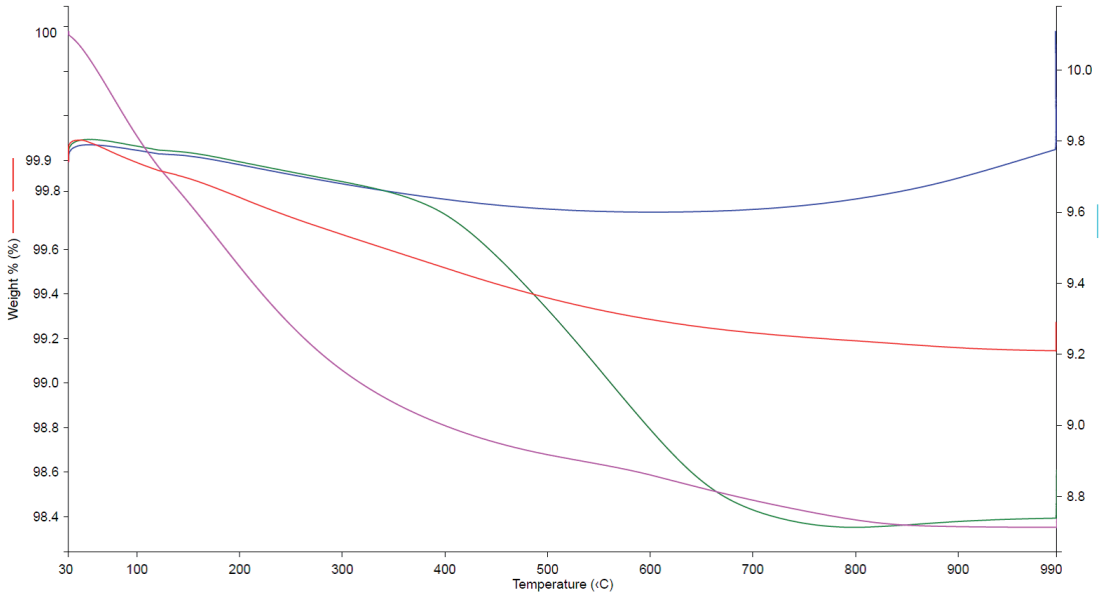

Fig. 3. TGA of the samples: CRT glass (red curve), slag (blue curve), fly ash (green curve), zeolite (purple curve).

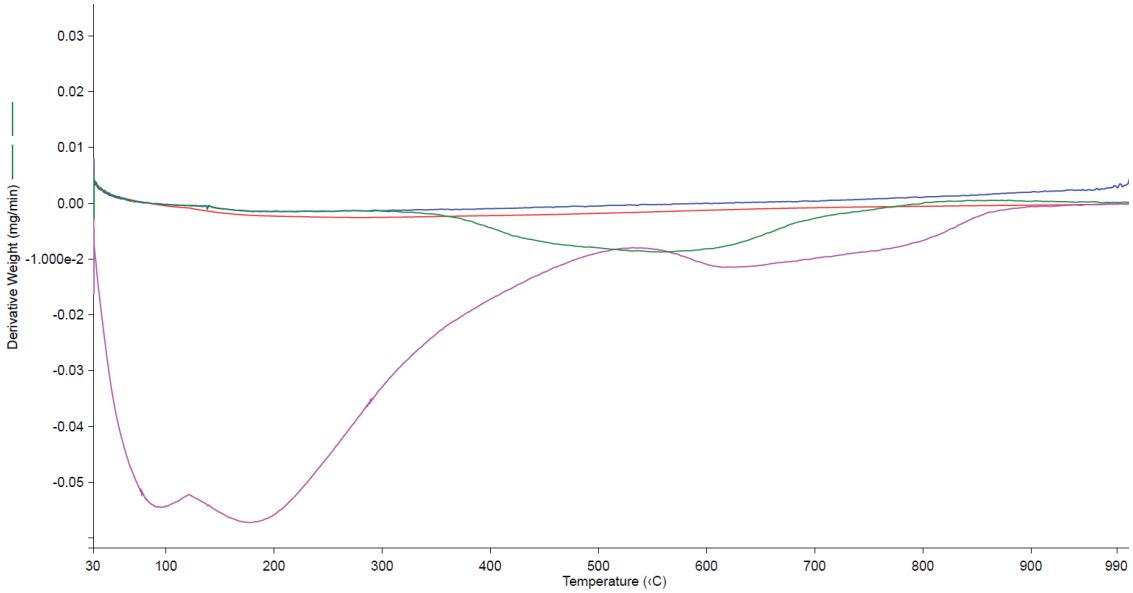

Fig. 4. DTG of the samples: CRT glass (red curve), slag (blue curve), fly ash (green curve), zeolite (purple curve).

distinct degradation phases. The first phase, occurring between 30-278ºC, is characterized by a 9.3% mass loss due to the evaporation of physically and chemically bound water [48]. The second phase, between 636ºC and 755ºC, involves an additional 4.4% mass loss, resulting in a final residual mass of 86.15% at 990ºC.

At approximately 900ºC, the system shows phase and thermal stability corresponding to the transformation that follows the degradation and recrystallization of the zeolitic structure. The conversion into an amorphous aluminosilicate phase enhances the material's reactivity and enables zeolite sinterability.

To evaluate the efficiency of the combined components, a TGA analysis was performed on a mixture composed of equal mass fractions of CRT glass, slag, fly ash, and zeolite.

The analysis was carried out under the same thermal conditions as the individual samples, simulating the actual sintering process (Fig. 5).

The TGA and DTG curves in Fig. 5 indicate degradation processes occurring in three distinct phases. The first phase, within the temperature range of 30ºC to 163ºC, corresponds to the evaporation of surface and adsorbed water, as well as the initial stages of dehydroxylation, suggesting the presence of porous and hygroscopic components in the system.

The second phase, between 163ºC and 455ºC, involves the release of bound water and volatile compounds, along

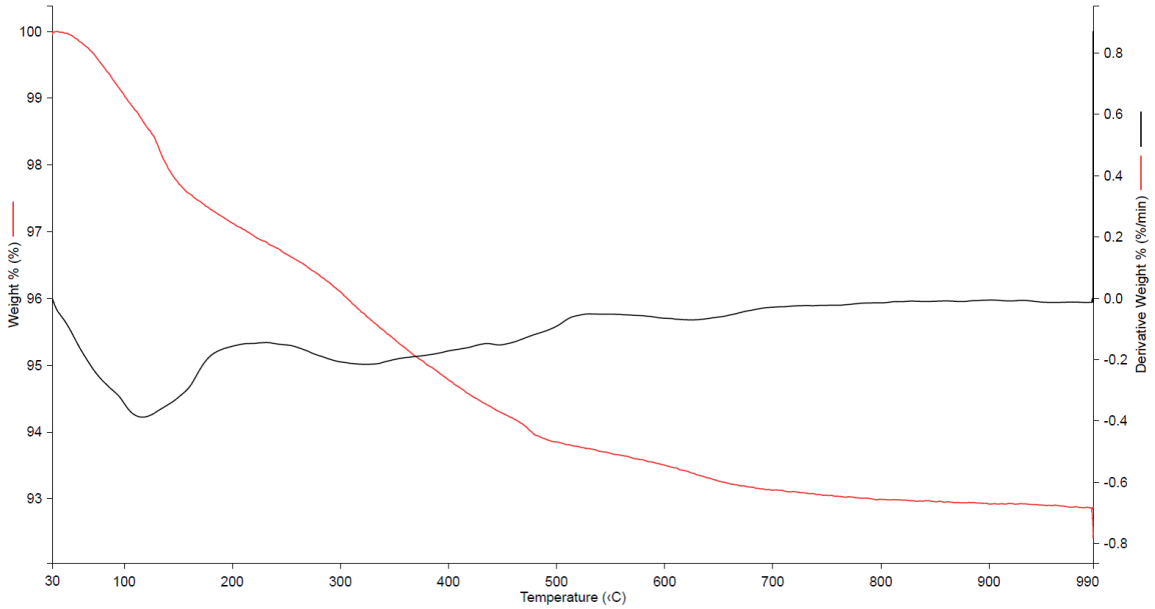

Fig. 5. TGA (red curve) and DTG (black curve) of the component mixture.

with the onset of inter-component reactions, during which solid sintered phases begin to form.

The DTG peak observed at 306.07ºC indicates the activation of pozzolanic reactions, indicating the chemical reactivity of the system. The third phase, spanning from 455ºC to 494ºC, is associated with the stabilization of surface characteristics, while the DTG peak at 473.97ºC marks the onset of fusion and formation of sintered phases – critical steps in the development of a compact and stable material.

In terms of composite mixture reactions, the identified thermal peaks (e.g., at 306ºC and 473ºC) can be associated with pozzolanic activation and the initiation of fusion, both of which are key to the formation of a dense sintered phase. These findings are consistent with previous studies that have identified these temperature ranges as critical for the development of solid phases in fly ash- and slag-based materials [49].

Importantly, no further mass loss was recorded above 750ºC, indicating the phase and thermal stability of the system. According to previous research, the authors demonstrated that fly ash and slag-based geopolymers exhibit high stability above 700ºC, with negligible mass loss – findings that align with the results of this study [50, 51]. The high residual mass at 990ºC (92.87%) confirms that the majority of the system remains inert at elevated temperatures, further supporting the suitability of these components for sintering applications. This thermal behavior contributes to process reliability and energy efficiency, providing a foundation for the development of sustainable and functional sintered materials.

The TGA analysis of the mixture demonstrates a synergistic effect among the components, with controlled mass losses and stable thermal behavior across a broad temperature range. The degradation proceeds in distinct phases corresponding to individual components, without undesirable interactions. The thermal stability of the mixture up to 990ºC confirms its suitability for sintering processes, with optimized reactivity and phase transformations.

CRT glass, rich in silicon dioxide, ensures phase coherence and structural stability; slag and fly ash contribute pozzolanic and hydraulic properties, while zeolite, owing to its porous aluminosilicate structure and ionic characteristics, enhances the homogeneity and thermal compatibility of the system.

Comparative Context, Sinterability Assessment, and Benchmarking

To appraise the physical properties of the obtained sintered material, an approximate (indirect) analysis of composition-based indicators was performed – basicity (B), silica modulus (SM), network former/modifier ratio (NFM), and the rule-of-mixtures (ROM) theoretical density – for each constituent and for the equal-mass blend (Table 2).

Table 2 shows that the constituents occupy complementary compositional roles: CRT glass is strongly network-former–rich (B = 0.028; SM = 3.811; NFM = 3.848), acting as a glassy flux; slag is modifier-dominated (B = 1.33; SM = 0.588; NFM = 0.729), favoring Ca/Mg-silicate formation; fly ash adds additional network formers (B = 0.136; SM = 4.419; NFM = 3.086); and zeolite is the most network-former–rich (B = 0.11; SM = 5.868; NFM = 6.473). As a result, the equal-mass blend falls in an intermediate regime (B = 0.275; SM = 2.325; NFM = 2.439), balancing viscous flow (from the glassy fraction) with Ca-silicate skeleton formation (from slag) while maintaining network stability (from fly ash and zeolite).

Table 2. Derived indices (B, SM, NFM) and ruleofmixtures density for each constituent and for the equalmass blend (computed from normalized XRF oxides).

Material	B (basicity)	SM (silica modulus)	NFM (network former/modifier)	ROM density (g/cm³)
CRT glass	0.028	3.811	3.848	2.639
Slag	1.33	0.588	0.729	3.127
Fly ash	0.136	4.419	3.086	3.129
Zeolite	0.11	5.868	6.473	2.847
Mixture (25:25:25:25)	0.275	2.325	2.439	2.921

Combining CRT glass, slag, fly ash, and zeolite therefore yields compositional and functional complementarity that is not typically achieved with individual constituents alone: Ca/Mg-rich basic oxides (predominantly from slag) act as network modifiers and promote Ca/Mg-silicate formation; a SiO_2-rich glassy fraction (CRT) provides phase mediation and viscous flow; reactive aluminosilicates (fly ash) aid network formation and distribute reaction nuclei; and a porous aluminosilicate framework (zeolite) transforms after dehydration into a more reactive amorphous phase that stabilizes the silicate network.

Upon heating, this role distribution produces a synergistic densification mechanism: removal of surface/structurally bound H_2O at low temperature (dominated by zeolite), reactions between the glassy phase and Ca/Mg-rich components at intermediate temperatures, and liquid-phase sintering governed by the silicate matrix at higher temperatures. The stable sintering region quantified by TGA (~750-990ºC) indicates that these transformations proceed without additional gas evolution, reducing the risk of gas-induced porosity and enabling controlled densification. The mid-range indices of the blend are consistent with this balanced behavior.

Prior studies generally examine single-stream or binary systems, e.g., CRT glass with aluminosilicate precursors [11, 22], slag-based ceramics [26, 27], or fly-ash geopolymers/ceramics [50, 51]. In these reports, CRT-based systems lower effective sintering temperatures via fluxing action (stable sintering region quantified by TGA ~800-900ºC) but may risk excessive flow without modifiers; slag-based ceramics densify strongly via Ca/Mg-silicates but often at higher optimal temperatures (≥1000-1200ºC); fly-ash systems emphasize network formers with high thermal stability (≥700ºC) and modest mass loss, yet may require modifiers for rapid densification. Against this background, the present quaternary blend exhibits intermediate B, SM, NFM and a negligible-loss stable sintering region quantified by TGA of ~750-990ºC, indicating controlled densification with lower gas-porosity risk, consistent with the qualitative behaviors reported in [11, 22, 26, 27, 50, 51], but achieved here within a single, integrated system.

The indicators in Table 2 point to a "golden mean" between flowability and network stability: there are sufficient modifiers for diffusion and pore closure alongside sufficient network formers to preserve silicate-network integrity. The formulation is also robust to typical compositional variability of industrial by-products while allowing fine-tuning of component ratios to target performance (e.g., lower porosity or higher thermal stability) within the selected regime. These indices are widely used in ceramic and glass science to compare compositional variations, providing a concise means of assessing network connectivity and the technological behavior of sintered products [22, 23].

The strengths of this study stem from an integrated four-stream formulation (CRT glass, slag, fly ash, zeolite) that unifies complementary roles typically treated separately in the literature, and from a transferable proxy framework – linking B, SM, NFM, ρ with the stable sintering region quantified by TGA – that enables composition-to-process mapping and application-oriented guidance on sinterability. Together with the benchmarking above, these features establish a practical design logic connecting flux-assisted viscous flow (CRT), Ca-silicate skeleton formation (slag), and network stabilization (fly ash, zeolite) within a single waste-derived formulation, supporting energy-efficient sintering and robust processing.

Conclusions

This study confirms the potential of industrial by-products – CRT glass, slag, and fly ash – and natural zeolite for sintering routes toward functional and sustainable materials. The high SiO_2 content across all constituents favors network formation and reactivity, while CaO from slag contributes hydraulic character and phase stability. Owing to its porosity and ion-exchange capacity, zeolite further enhances sinterability and functional response. The integrated XRF, FTIR, SEM, and TGA analysis indicates that the selected combination can be sintered at comparatively lower temperatures with negligible mass loss and preserved structural integrity – key factors for energy-efficient processing. Environmentally, diverting these waste

streams from landfills reduces the demand for primary raw materials and supports circular economy objectives. Lower sintering temperatures further contribute to energy savings and reduced greenhouse-gas emissions, strengthening the sustainability profile of the proposed formulation. Specific directions for future research (targeted optimization and validation):

Optimization of component ratios (mixture design):

– Explore a constrained simplex of CRT glass (~15-40 wt%), slag (~20-50 wt%), fly ash (~15-40 wt%), and zeolite (~5-25 wt%) in 5 wt% increments.
– Target composition indices B ≈ 0.25-0.60, SM ≈ 1.8-3.0, NFM ≈ 2.0-2.8 to balance fluidity (modifiers) and network stability (formers).
– Sintering atmosphere and schedule:
– Test inert (N_2) as a reference alongside O_2 atmospheres to control oxidation states and phase equilibria.
– Map schedules 800-1000ºC, dwell 30-120 min, heating rate 5-15ºC/min.
– Align the selected temperature range with the stable sintering region quantified by TGA.
– Property validation aligned with applications:
– Perform XRD (Rietveld) quantification of crystalline transformations suggested by FTIR and TGA to strengthen cross-validation.
– Where relevant, conduct leaching tests (heavy metals) to evaluate environmental safety.

Acknowledgments

This work was supported by the Agreement on the Implementation and Financing of Scientific Research Work, Registration Number: 451-03-137/2025-03/200148.

Conflict of Interest

The authors declare no conflict of interest.

References

1. MORSELETTO P. Targets for a circular economy. Resources, Conservation & Recycling. **153**, 104553, **2020.**
2. LIEDER M., RASHID A. Towards circular economy implementation: A comprehensive review in context of manufacturing industry. Journal of Cleaner Production. **115,** 36, **2016.**
3. POLICY COMMONS. Available online: https://coilink.org/20.500.12592/wr5sc0, (accessed on 11 July 2025).
4. ZHANG J., FAN Y., ZHAI X., KUMAR V.V. Investigating the effects of sintering additives and heating regimes on the performances of glass–ceramic proppants derived from industrial wastes. Materials & Design. **250**, 11363, **2025**.
5. ZHOU S., LIU G., WANG C., ZHANG Y., YAN C., SHI Y. Thermal debinding for stereolithography additive manufacturing of advanced ceramic parts: A comprehensive review. Materials & Design. **238**, 112632, **2024**.
6. HUA X., GAO Z., SHI Y., HAO W., LIU X., LI R. Transforming industrial solid wastes into eco-friendly zeolite material for efficient heavy metal ion stabilization through host-guest combination. Chemical Engineering Research and Design. **196**, 656, **2023**.
7. GRIFASI N., ZIANTONI B., FINO D., PIUMETTI M. Fundamental properties and sustainable applications of the natural zeolite clinoptilolite. Environmental Science and Pollution Research. **2024**.
8. SONG W., ZOU D., LIU T., TENG J., LI L. Effects of recycled CRT glass fine aggregate size and content on mechanical and damping properties of concrete. Construction and Building Materials. **202**, 332, **2019**.
9. EFTIMIE M., TACU I. Experiments to obtain glass-ceramics from glass waste resulted from cathode ray tubes-CRT. Romanian Journal of Materials. **44** (2), 124, **2014**.
10. REBEN M., KOSMAL M., ZIĄBKA M., PICHNIARCZYK P., GRELOWSKA I. The influence of TiO_2 and ZrO_2 on microstructure and crystallization behavior of CRT glass. Journal of Non-Crystalline Solids. **425**, 118, **2015**.
11. LU X., YANG J., NING X., SHIH K., WANG F. Crystallization pathways in glass-ceramics by sintering cathode ray tube (CRT) glass with kaolin-based precursors. Journal of the European Ceramic Society. **38** (15), 5184, **2018**.
12. LI G., LIU P., CHAO S., ZHANG X., LI J., ZHANG Y., DUAN Y. The mineral phase evolution characteristics and hydration activity enhancement mechanism of steel slag under NaOH alkaline excitation. Journal of Alloys and Compounds. **978**, 173524, **2024**.
13. WANG Y., JIANG B., SU Y., HE X., WANG Y., OH S. Hydration and compressive strength of activated blast-furnace slag-steel slag with Na_2CO_3. Materials. **15** (13), 4375, **2022**.
14. ZHAO Z., ZHANG C., LI J., WANG W., ZHAO H., LI Y., LUO J. Sintering conversion to porous diopside ceramic from geopolymer fabricated by iron tailings and steel slag. Ceramics International. **51** (12), 15687, **2025**.
15. XU L., WANG Y., LI X., LIU Y., CHEN M. Sintering, microstructure and mechanical properties of anorthite-based ceramics prepared from iron-extracted steel slag. Journal of Alloys and Compounds. **1005**, 176221, **2024**.
16. LI R., XIE Z., ZHOU Y., WANG W., GUI X. Fly ash as a high-capacity, high-rate performance, and low-cost cathode material for lithium-sulfur batteries. Journal of Power Sources. **640**, 236738, **2025**.
17. ZHUANG X.Y., CHEN L., KOMARNENI S., ZHOU C.H., TONG D.S., YANG H.M., YU W.H., WANG H. Fly ash-based geopolymer: clean production, properties and applications. Journal of Cleaner Production. **125**, 253, **2016**.
18. OROZCO C., TANGTERMSIRIKUL S., SUGIYAMA T., BABEL S. Examining the endpoint impacts, challenges, and opportunities of fly ash utilization for sustainable concrete construction. Scientific Reports. **13** (1), 18254, **2023**.
19. BEHERA S.K., SAHOO K.K., BHOSALE A., PRADHAN A. Structural properties and temperature effect of sintered fly ash pellets concrete. Materials Today: Proceedings. **2023**.
20. ALGIERI C., DRIOLI E. Zeolite membranes: synthesis and applications. Separation and Purification Technology. **278**, 119295, **2021**.

21. SANTRA N., KAYAL N. Preparation of high performance porous SiC ceramic membrane support using zeolite and alumina as sintering additives. Materials Science and Engineering: B. **303**, 117311, **2024**.
22. LONG W.J., ZHANG X., XIE J., KOU S., LUO Q., WEI J., LIN C., FENG G.L. Recycling of waste cathode ray tube glass through fly ash-slag geopolymer mortar. Construction and Building Materials. **322**, 126454, **2022**.
23. PAUZI N.N.M., ABIDIN A.Z., ZAIN M.F.M. Characterization of spherical waste CRT glass as aggregates in concrete. International Journal of Advanced Research in Engineering Innovation. **2** (3), 1, **2020**.
24. LIU J., JIANG W., CHENG D., ZHONG Q., LIU C., JIANG Y., ZHU J., ZHANG H., XU L., MA X. Effect of silica content on iron ore sintering. Metals. **13** (6), 1009, **2023**.
25. CHIANG P.C., PAN S.Y. Iron and steel slags. In book: Carbon Dioxide Mineralization and Utilization. Springer: Berlin, Germany. 233, **2017**.
26. ARKAME Y., HARRATI A., JANNAOUI M., ET-TAYEA Y., YAMARI I., SDIRI A., SADIK C. Effects of slag addition and sintering temperature on the technological properties of dolomite based porous ceramics. Open Ceramics. **13**, 100333, **2023**.
27. RAHOU J., REZQI H., EL OUAHABI M., FAGEL N. Characterization of Moroccan steel slag waste: the potential green resource for ceramic production. Construction and Building Materials. **314**, 125663, **2022**.
28. ALTERARY S., MAREI N. Fly ash properties, characterization, and applications: A review. Journal of King Saud University - Science. **33** (6), 101536, **2021**.
29. DERBE T., TEMESGEN S., BITEW M. A short review on synthesis, characterization, and applications of zeolites. Advances in Materials Science and Engineering. **2021** (1), 1, **2021**.
30. RAMEZANI H., AZIZI S.N., CRAVOTTO G. Improved removal of methylene blue on modified hierarchical zeolite Y: achieved by a "destructive-constructive" method. Green Processing and Synthesis. **8**, 730, **2019**.
31. BACAKOVA L., VANDROVCOVA M., KOPOVA I., JIRKA I. Applications of zeolites in biotechnology and medicine - a review. Biomaterials Science. **6** (5), 974, **2018**.
32. FARAG M.A., IBRAHIM A., HASSAAN M.Y., RAMADAN R.M. Enhancement of structural and optical properties of transparent sodium zinc phosphate glass-ceramics nanocomposite. Journal of the Australian Ceramic Society. **58**, 653, **2022**.
33. AZIZ A., STOCKER O., EL HASSANI I.E.E.A., LABORIER A.P., JACOTOT E., EL KHADIRI A., EL BOUARI A. Effect of blast-furnace slag on physicochemical properties of pozzolan-based geopolymers. Materials Chemistry and Physics. **258**, 123880, **2021**.
34. FELAOUS K., AZIZ A., ACHAB M. Physico-mechanical and durability properties of new eco-materia l based on blast furnace slag activated by Moroccan diatomite gel. Environmental Science and Pollution Research. **30**, 3549, **2023**.
35. PULIGILLA S., MONDAL P. Co-existence of aluminosilicate and calcium silicate gel characterized through selective dissolution and FTIR spectral subtraction. Cement Concrete Research. **70**, 39, **2015**.
36. ĐORĐEVIĆ D., STANKOVIĆ M., KRSTIĆ N., DIMITRIJEVIĆ V., ANASTASIJEVIĆ N., ĐORĐEVIĆ M., NIKOLIĆ M. Geochemical analysis of Kostolac power plant fly ash: working and living environment influence aspect. Safety Engineering. **8** (1), 15, **2018**.
37. HE X., YAO B., XIA Y., HUANG H., GAN Y., ZHANG W. Coal fly ash derived zeolite for highly efficient removal of Ni^{2+} in wastewater. Powder Technology. **367**, 40, **2020**.
38. GHADAMNAN E., NABAVI S.R., ABBASI M. Nano LTA zeolite in water softening process: synthesis, characterization, kinetic studies and process optimization by response surface methodology (RSM). Journal of Water and Environmental Nanotechnology. **4** (2), 119, **2019**.
39. MELANINGTYAS G.S.A., KRISNANDI Y.K., EKANANDA R. Synthesis and characterization of NaY zeolite from Bayat natural zeolite: effect of pH on synthesis. Materials Science and Engineering. **496**, 012042, **2019**.
40. MALCHIODI B., SILIGARDI C., POZZI P. Unsaturated polyester-based polymer concrete containing recycled cathode ray tube glass aggregate. Journal of Composites Science. **6** (2), 47, **2022**.
41. LESNIKOV A.K., LESNIKOV P.A., TYURNINA Z.G. Glass ceramics based on silicon dioxide as a promising material for use in nuclear power engineering. Glass Physics and Chemistry. **48**, 285, **2022**.
42. SETHUPATHY G., MADHAN M B., GOTUR S., ARUN A., NAIR D. Analysis of complete replacement of river sand by Iron ore slag sand. International Research Journal of Engineering and Technology (IRJET). **5** (5), 3940, **2018**.
43. AKHIL NAVDEEP S. Microstructural characteristics of iron-steel slag concrete: A brief review. Materials Today: Proceedings. **2023**.
44. JEYAGEETHA C., KUMAR P.K. Study of SEM/EDXS and FTIR for fly ash to determine the chemical changes of ash in Marine environment. International Journal of Science and Research (IJSR). **5** (7), 1688, **2015**.
45. ISOPENCU G., EFTIMIE M., MELINESCU A., DANCILA A.M., MARES M. Recycling of glass waste by deposition of TiO_2 for the intensification of the photocatalytic effect in the purification of wastewater. Coatings. **12** (11), 1794, **2022**.
46. BARTOŇOVÁ L. Unburned carbon from coal combustion ash: An overview. Fuel Processing Technology. **134**, 136, **2015**.
47. ŠEŠLIJA M., ROSIĆ A., RADOVIĆ N., VASIĆ M., ĐOGO M., JOTIĆ M., Laboratory testing of fly ash. Technical Gazette. **23** (6), 1839, **2016**.
48. KRÓL M.K., JELEŃ P. The effect of heat treatment on the structure of zeolite A. Materials. **14** (16), 4642, **2021**.
49. SNELLINGS R., SCRIVENER K. Rapid screening tests for supplementary cementitious materials: past and future. Materials and Structures. **49**, 3265, **2016**.
50. ZHANG H. Y., KODUR V., WU B., CAO L., QI S.L. Comparative thermal and mechanical performance of geopolymers derived from metakaolin and fly ash. Journal of Materials in Civil Engineering. **28** (2), 04015092, **2016**.
51. ZHAO J., WANG K., WANG S., WANG Z., YANG Z., SHUMUYE E.D., GONG X. Effect of elevated temperature on mechanical properties of high-volume fly ash-based geopolymer concrete, mortar and paste cured at room temperature. Polymers. **13** (9), 1473, **2021**.